

Lifetime of image-potential states on metal surfaces

S. Schuppler, N. Fischer, Th. Fauster, and W. Steinmann

Sektion Physik, Universität München, Schellingstrasse 4, W-8000 München 40, Germany

(Received 6 July 1992)

High-resolution bichromatic two-photon photoemission spectroscopy was used for an investigation of intrinsic linewidths and, thus, lifetimes of image-potential states on clean and adsorbate-covered metal surfaces. The linewidths of the first image state are 16 ± 4 and 70 ± 8 meV for Cu(111) and Ni(100), respectively. Together with the results for Ag(100) and Ni(111) published previously, a systematic comparison with theoretical predictions is presented. The discrepancies between experiment and theory can be understood qualitatively if the actual band structure is taken into account. A high density of unoccupied bulk or surface states offers many channels for the decay of the image state via electron-hole pair production and results in the large linewidth observed on the nickel surfaces. The opposite is found for Cu(111) where the band gap extends below E_F . For oxygen adsorption on Ni(100), an increase of the linewidth is observed, which can be explained by the lateral confinement of the image state and inelastic scattering by the adsorbate atoms.

I. INTRODUCTION

Electrons can be trapped by the image potential in front of a metal surface if the electron reflectivity of the metal is high for energies below the vacuum energy E_{vac} . A high electron reflectivity obviously occurs in a gap of the projected bulk band structure, a situation that is sketched in Fig. 1(a). The long-range $1/z$ form of the image potential leads to a series of unoccupied electronic states that converge toward E_{vac} and are called image states. The binding energies E_b are referred to E_{vac} and to a first approximation exhibit a Rydberg-like behavior: $E_b(n) \approx 1/16n^2$ Ry. On metals, image states were first detected experimentally by low-energy electron-diffraction (LEED) fine-structure analysis¹ and could be observed in a more direct way in inverse photoemission (IPE) (Refs. 2–4) and two-photon photoemission (2PPE).^{5,6} Whereas resolution in IPE is currently limited to about 260 meV (Refs. 7 and 8) in energy and about 0.05 \AA^{-1} in momentum, 2PPE is superior in both respects. Recent 2PPE experiments have demonstrated an energy resolution of ≈ 30 meV (Refs. 9 and 10) and an angular resolution of $\approx 0.007 \text{ \AA}^{-1}$.¹¹ This makes 2PPE a suitable tool for precise measurements of unoccupied states.

Binding energies and effective masses of image states can be understood qualitatively by the so-called phase analysis model,¹² which combines a multiple-reflection description of the image state¹³ with a two-band model approximating the crystal reflectivity. According to this model, the binding energy of the image-state series depends on the position of E_{vac} relative to the band gap. Since the band gap on a fcc (100) surface is located at higher energies than for the corresponding (111) surface, the binding energies of the Rydberg series should be smaller for the former.¹² This trend could indeed be observed in 2PPE experiments.¹⁴

Image states are expected to have long lifetimes. This

is because they are located mainly in front of the surface, which keeps the overlap between the image-state wave function and metal wave functions relatively small. Experimentally lifetimes of image states have only recently become accessible through time-resolved^{15–17} and energy-resolved two-photon photoemission.^{9,10} In energy-resolved 2PPE the intrinsic linewidth Γ is measured, which is related to the lifetime τ via the uncertainty principle $\Gamma\tau = \hbar$, and intrinsic linewidths for the $n=1$ state between 0.02 and 0.08 eV were found. Since bulk states of comparable energy (≈ 4 eV above E_F) exhibit a

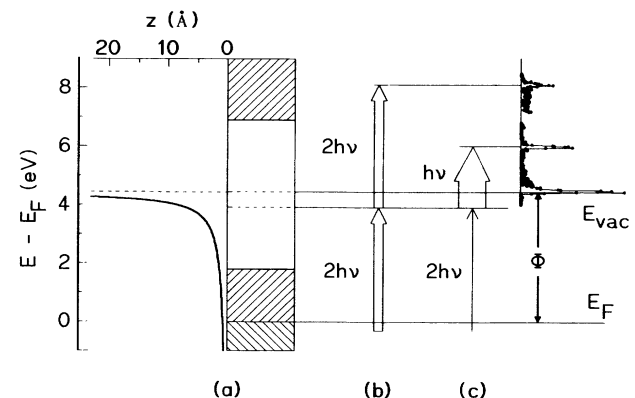


FIG. 1. Image states and two-photon photoemission. (a) Image potential in front of the surface and projected bulk band structure for $k_{\parallel}=0$ (i.e., the $\bar{\Gamma}$ point of the surface Brillouin zone). The band gap shown is that of Ag(100). (b) Energy scheme of conventional 2PPE with the first image state as the intermediate state. (c) Same as (b), but bichromatic 2PPE. Conventional 2PPE utilizes frequency-doubled laser light (" $2h\nu$ ") for both excitation steps, whereas in bichromatic 2PPE the second excitation is performed with the ground wave (" $h\nu$ ") of the laser. The widths of the arrows symbolize light intensities. The energy distribution curve in the upper right shows the peaks corresponding to both excitation schemes.

linewidth around 0.5 eV,¹⁸ these results underline the basic picture of image states as states that are effectively decoupled from the bulk.

A thorough understanding of image states must be based on a many-body description of the complex self-energy at the surface (e.g., by means of Green's functions^{19,20}), which incorporates the dynamic response of the metal surface on the field of an electron outside the metal. The effective surface potential can be derived from the *real part* of the electron self-energy. In this way both the correct imagelike $1/z$ behavior far from the surface as well as a continuously differentiable transition from the surface potential to the bulk potential is obtained. Solving Schrödinger's equation (in a self-consistent way) yields the binding energy of the image states which can then be compared to experiment. The same formalism describes the linewidth of image states through the *imaginary part* of the self-energy. Thus measurements of lifetimes establish an additional and independent test for calculations of the self-energy and the underlying theoretical assumptions. This provides strong motivation for attacking the difficult task of measuring lifetimes of image states.

The paper is organized as follows: First we give a short overview of the present theoretical models and results for the lifetimes of image states. The experimental section contains details of the high-resolution 2PPE experiment and the determination of the intrinsic lifetime broadening from the data. In Sec. IV we present the spectra for the surfaces Cu(111) and Ni(100), which allow a determination of the lifetimes of image states. Section V is devoted to a systematic comparison between the experimental results—including our earlier results on Ag(100) (Ref. 9) and Ni(111) (Ref. 10)—and the theoretical predictions. We close with a short comment about to what extent electrons in image states can form a two-dimensional electron gas.

II. THEORETICAL ESTIMATES OF IMAGE STATE LIFETIMES

Up to now quantitative predictions of lifetimes of image states on metal surfaces have been given solely in the papers of Echenique and coauthors.^{13,19,21–24} The decay is dominated by electron-hole pair production, a process which is included in the self-energy formalism to be discussed in this section.

In Refs. 19, 22, and 23 a *GW* approximation²⁵ is used for calculating the imaginary part of the electron self-energy. The *GW* approximation has been shown to be quite successful in many areas, e.g., band gaps in semiconductors and insulators, and the electronic structure of defects. However, constructing reasonable Green's functions and screened interactions at a surface is far from being trivial. Indeed, Echenique and co-workers had to invoke several truncations in the course of their calculations:

(i) First they approximate the noninteracting one-electron Green's function G_0 (which is used instead of the full G throughout) in the jellium model. Thus the actual band structure is neglected.

(ii) The surface dielectric function (surface DEF) which enters the calculation of the screened interaction W is determined approximately from a bulk DEF using mainly the semiclassical infinite barrier model of Ref. 26. For the bulk DEF the Lindhard DEF (Ref. 27) is used, which describes the response of a homogeneous electron gas, thus neglecting any band structure effect on W as well.

(iii) In addition, the z -dependent part of the wave function of the image state which is needed for calculating the expectation value of the self-energy is taken to be hydrogenic in the vacuum and approximated by a two-band model in the crystal. This is not likely to be very realistic in the surface region, where the effective surface potential differs most from the diverging image potential.

Within these approximations Echenique and co-workers quantify the intuitive expectation that a larger penetration depth causes a shorter lifetime. They use the fact that the penetration depth of the image-state wave function into the bulk is mainly determined by the energetic position of the image state in the band gap. For the $n=1$ state near the middle of the gap the penetration is small and may even be neglected altogether. This is the case for Ag(100), where a lifetime broadening of about 5 meV full width at half maximum (FWHM) (and 8 meV with a somewhat better approximation for the surface DEF) has been calculated.¹⁹ For surfaces where the first image state is close to the band-gap edge and penetration is therefore significant—like on Cu(111) and Ag(111)—they calculate linewidths of 19 [Cu(111)] and 22 meV [Ag(111)] for 10% penetration, and linewidths of 39 [Cu(111)] and 43 meV [Ag(111)] for 20% penetration.²² In that work the authors assign a 10% penetration to Cu(111) and about a 20% penetration to Ag(111). These values, however, are quite doubtful since even slight deviations in the position of the $n=1$ state relative to E_F and the upper band-gap edge from the values they assume can alter the picture substantially. We believe that fairly recent experimental results indicate a greater penetration on Cu(111) than on Ag(111):

(i) On Ag(111) the earlier reference value for the work function $\Phi=4.74$ eV had to be corrected to 4.56 eV.²⁸ This means that the $n=1$ state lies further away from the upper band-gap edge than assumed previously [3.79 eV above E_F , while the upper band-gap edge is around 4.0 eV above E_F (Ref. 29)].

(ii) On Cu(111) the upper band-gap edge may lie lower than the value cited in Ref. 29. In Ref. 30 a value of 4.1 instead of 4.25 eV above E_F is reported, which means that the $n=1$ state (4.10 eV above E_F) is located directly at the band-gap edge.

Measurements of the dispersion of the first image state on both surfaces support this view: On Cu(111) the effective mass is $m^*/m_e=1.0$,³¹ whereas on Ag(111) it was found to be 1.3.³² According to the phase analysis model^{31,32} this can be understood if the $n=1$ state on Cu(111) is located very close to (or even above) the upper band-gap edge, whereas the state on Ag(111) must be more separated from the gap edge. From this information the reverse assignment for the penetration of 20% [Cu(111)] and 10% [Ag(111)] is much more plausible, which gives a conservative estimate for the intrinsic

linewidth on Cu(111) of 40 meV [the one on Ag(111) is then around 20 meV].

Since the calculated linewidths depend almost exclusively on penetration and only marginally on the material, we use them to find a rough estimate for the linewidths of the image states on nickel surfaces. The image states are located slightly above and below the center of the band gap on Ni(111) and Ni(100), respectively. Therefore we expect linewidths around 15 meV, which is between the values for Ag(100) and Ag(111).

Keeping in mind that the present theory should be taken *cum grano salis* since it assumes a free-electron-like behavior of the metal, we summarize its predictions as follows:

(i) Image states become more long-lived with increasing n , as long as they fall inside the band gap. An image state located outside the band gap is broadened substantially due to the direct coupling to energetically degenerated bulk states [about 50 meV for $n=2$ for Cu(111) and Ag(111) (Ref. 22)].

(ii) By far the most important parameter determining the lifetime of an image state is its penetration depth into the bulk. The penetration depth is greatest for the image state near the band-gap edge and least for one near the middle of the band gap. Experimental realizations for these extreme cases are Ag(100) and Cu(111). The lifetime for Ag(100) is expected to be several times larger than the value for Cu(111).

(iii) Numerically linewidths between 8 and 40 meV are expected for copper and silver (100) and (111) surfaces. From their position in the band-gap image states on nickel surfaces should have widths around 15 meV.

III. EXPERIMENT

A. Bichromatic 2PPE

In a 2PPE process an electron from an occupied state below E_F is excited by a photon into an unoccupied state above E_F . If a second photon arrives within the lifetime of the excited state, the electron may be lifted above the vacuum level E_{vac} where it can be analyzed like in ordinary photoemission. This situation is depicted in Figs. 1(b) and 1(c).

The photon energies of the two excitation steps may be different. Whereas the first step must be performed with an energy sufficient to reach the image state at 3.8–4.5 eV above E_F , thus requiring UV photons, much less energy is needed in the second step for ionization. The UV light causes photoemission from thermally occupied states above E_F .^{9,33} For high UV intensities this leads to an increased spectral background, and 2PPE can be disturbed substantially by a Gaussian broadening of the peaks and shifts of their positions. Choosing a much smaller second photon energy and increasing its intensity at the expense of the UV intensity should therefore lead to an increased signal-to-noise ratio (SNR). It turns out experimentally⁹ that this “bichromatic” excitation indeed enhances the SNR by an order of magnitude, thus enabling us to investigate weak structures more precisely.

B. Experimental setup

The basic experimental setup for 2PPE experiments has been described elsewhere (Ref. 6 and references therein). The light source is an excimer-laser-pumped three-stage dye laser which was tuned for the experiments reported here between $h\nu=2.10$ – 2.82 eV. By frequency doubling in a β -BaB₂O₄ crystal³⁴ we obtained the necessary photon energy for the first excitation step in the 2PPE process. In our experiment p polarization was needed for both excitation steps. Since in this type of frequency doubling the $2h\nu$ wave is polarized perpendicular to the ground wave $h\nu$, we used a set of two polarizers to adjust the intensity ratio and to turn both waves into p polarization. The laser light is focused onto the sample by achromatic UV-grade optics.

The electrostatic sectoral hemispherical energy analyzer combined with three-lens entrance and exit electron optics is capable of an energy resolution better than 30 meV and an angular resolution of about $\pm 0.6^\circ$. At typical kinetic energies of the emitted photoelectrons (2 eV) the angular resolution is equivalent to a k_{\parallel} resolution of 0.007 \AA^{-1} . Assuming a free-electron-like dispersion of the image state, this leads to an apparent broadening of the image state in the spectra well below 1 meV for normal emission. Throughout this work the electrons emitted perpendicular to the surface ($k_{\parallel}=0$) were detected.

The analyzer function can be well approximated by a Gaussian (see, e.g., Ref. 35). The intrinsic, lifetime-induced broadening has a Lorentzian shape and the resulting line shape is a convolution of both. The line-shape analysis used a nonlinear least-squares fitting procedure with the proper statistical weighting of the least-squares sums. The positions, intensities, and intrinsic Lorentzian widths of the peaks were fitted. The analyzer resolution represented by the width of the Gaussian was independently checked by measurements of the low-energy cutoff of photoemission spectra. This procedure has recently been shown to work successfully for 2PPE data^{9–11} and was again applied in the following.

IV. RESULTS

Figure 2 shows typical 2PPE spectra of the materials under investigation. They are referred to the same energy scale so that binding energies and linewidths can be compared in a direct way. Apart from Cu(111) at least the first two image states on each surface were measured. Two important features concerning linewidths are immediately obvious from this figure: (i) The first image state on Cu(111) is by no means broader than that on Ag(100), quite contrary to the expectation from the evaluation of present theory in Sec. II; and (ii) the image states on both nickel faces are much broader than on Ag(100) and Cu(111), in contrast to the expectation from the simple extrapolation of the theoretical model. We are now going to discuss the experimental results separately for the various surfaces. The comparison between the different surfaces and the comparison to theory will be presented in Sec. V.

A. Cu(111)

On Cu(111) only the first image state appears in the figure, because on this surface the L_2-L_1 gap at $\bar{\Gamma}$ extends down to 0.85 eV below E_F . Thus no bulk states exist for a direct excitation of the image state with $2h\nu < \Phi$. However, the occupied ($n=0$) surface state with $E_F - E_b = 0.39$ eV lies in the band gap and can serve as the initial state for a very efficient resonant excitation into the $n=1$ state if the photon energy $2h\nu$ is tuned to the energy difference between both states.⁵ In agreement with earlier 2PPE measurements²⁸ we found $\Phi^{\text{Cu(111)}} = 4.93 \pm 0.03$ eV and $E_b^{n=1} = 0.83 \pm 0.03$ eV; thus resonance occurs at $2h\nu \approx 4.49$ eV. With the ordinary light intensities used in Bi2PPE a much higher signal than on Ag(100) was observed in resonance, whereas off-resonance almost no signal from the $n=1$ state could be detected. This explains why the first two image states on

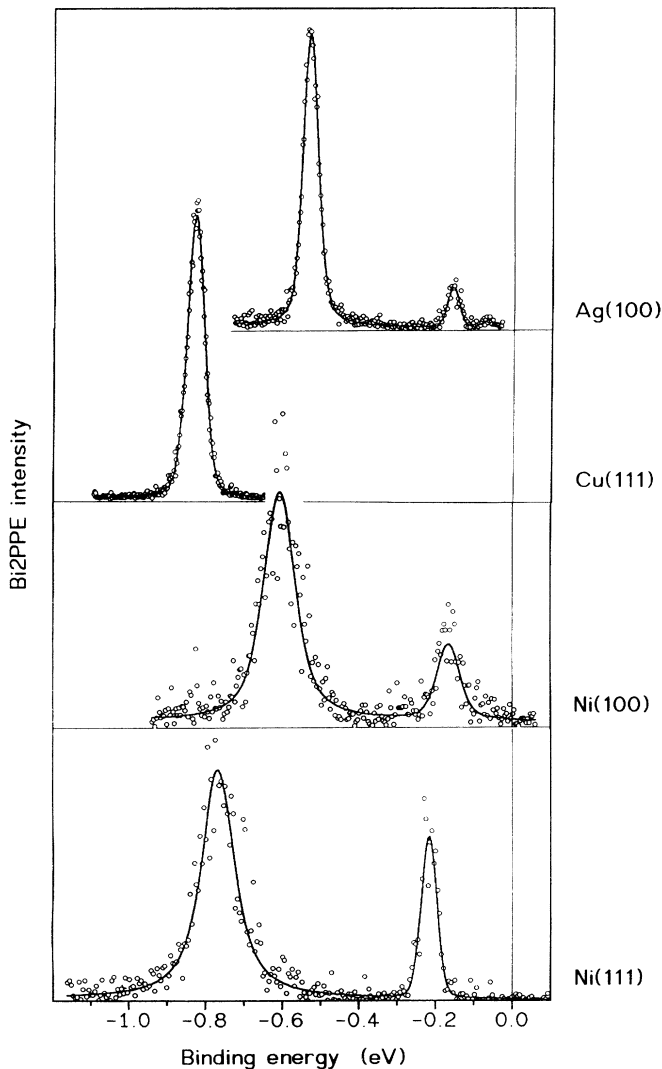


FIG. 2. Linewidth of the first image states on different metal surfaces. The binding energy is relative to E_{vac} . (a) Ag(100): $2h\nu = 4.350$ eV. (b) Cu(111): $2h\nu = 4.484$ eV (resonance with occupied surface state S_0). (c) Ni(100): $2h\nu = 5.061$ eV. (d) Ni(111): $h\nu = 5.102$ eV (monochromatic 2PPE).

Cu(111) could not be measured simultaneously. Line-shape analysis of spectra taken with different analyzer resolution (35–50 meV) gave in all cases within the error limits an intrinsic linewidth broadening of $\Gamma_1^{\text{Cu(111)}} = 16 \pm 4$ meV. This is even a slightly smaller linewidth than on Ag(100), where we found $\Gamma_1^{\text{Ag(100)}} = 21 \pm 4$ meV.⁹

It must be noted, however, that the intrinsic Lorentzian width obtained from line-shape analysis does not necessarily correspond to the lifetime of the intermediate state of the 2PPE process: It could be argued that if the excitation steps are coherent the lifetime of the hole left behind in the metal and that of the final state should be involved as well. (“Coherent” in this context stands for a phase correlation between the two excitation steps. It should not be confused with the coherency of the laser light used for the excitation.) In fact a simple second-order perturbation analysis shows that the Lorentzian width Γ appearing in the spectrum should then be $\Gamma = \Gamma_0 + 2\Gamma_1$, where Γ_0 denotes the lifetime broadening of the initial state and Γ_1 that of the intermediate state. Following the argument in Ref. 36 in this expression, the contribution from the width of the final state is already omitted since the intermediate state (being a surface state) has no k_{\perp} dispersion.

On Cu(111) the question of coherency can be tested rigorously by testing the relation $\Gamma = \Gamma_0 + 2\Gamma_1$. On this surface the $n=0$ surface state is, within our experimental conditions, the only possible initial state for exciting the $n=1$ state since it is located in a bulk band gap. Thus, by measuring its linewidth through single-photon photoemission, the lifetime broadening of the initial state in the 2PPE process is accessible directly and unambiguously. Using an argon resonance lamp we determined the intrinsic linewidth Γ_0 of the surface state to 54 ± 3 meV in agreement with earlier results.³⁷ However, the intrinsic Lorentzian width obtained from 2PPE spectra, 16 ± 4 meV, is much smaller than the width of the initial state, a fact which obviously rules out that the excitation steps are coherent. In other words, after the first excitation step the electron “forgets” about its initial state. An incoherent process is not surprising if the lifetime of the hole is much shorter than the lifetime of the image state. This holds even for Cu(111), where the occupied surface state has a very small intrinsic linewidth. For Ni(111) the occupied surface state is degenerate with bulk states and has a width around 400 meV.³⁸ On the (100) surfaces the initial states are bulk states which are expected to have shorter lifetimes than surface states due to their large penetration depth. Furthermore, we found the measured linewidths of the image-potential states to be independent of photon energy and thus the initial state. The $n=2$ image state shows in all cases a considerably narrower linewidth than the $n=1$ image state. For a coherent two-step excitation process the width would be $\Gamma_0 + 2\Gamma_2$, resulting in an unreasonably small linewidth for the initial state. Therefore it is safe to assume that on all surfaces studied in our work the 2PPE excitation is incoherent, and the measured Lorentzian widths are just the widths of the intermediate states in the excitation process, i.e., the widths Γ_n of the image states n .

B. Ni(100)

In this paper we report the first 2PPE measurements for this surface. We found it more difficult than on the other clean surfaces to obtain a reasonable SNR: For nickel the d bands lie in part above E_F , which leads to an especially high spectral background due to 1PPE (see above); furthermore, on a fcc (100) surface no occupied surface state exists which could be used for resonant excitation. This is an example where no quantitative results would have been possible at all without the bichromatic excitation process. The SNR can be improved still further by reducing the photon energy, but then the second image state can no longer be observed. Line-shape analysis of both types of spectra (with and without the $n=2$ state) yields the intrinsic linewidth of the first image state on Ni(100): $\Gamma_1^{\text{Ni}(100)} = 70 \pm 8$ meV. The second state is again narrower than the first, but due to the limited SNR no linewidth can be given.

We also give our results for the work function and binding energies of the first two image states on Ni(100): $\Phi^{\text{Ni}(100)} = 5.09 \pm 0.03$ eV; $E_b^{n=1} = 0.61 \pm 0.03$ eV; $E_b^{n=2} = 0.18 \pm 0.03$ eV. In much the same way as on Ni(111) (Ref. 10) we looked for a magnetic splitting of the $n=1$ state on Ni(100). We found that the splitting is not larger than 35 meV [compared to 40 meV on Ni(111)]. This upper limit is in good agreement with the value of 13 ± 13 meV from spin-resolved inverse photoemission.³⁹

C. Disordered adsorption

Upon adsorption of atoms on a clean surface the linewidth of image states increases. This can be seen in Fig. 3, where the additional linewidth broadening $\Delta\Gamma$ of the first image state on Ni(100) is plotted versus the work-function increase induced by submonolayer oxygen adsorption. For this system a linear dependence of the work-function increase $\Delta\Phi$ on the coverage Θ for coverages below 0.25 monolayers (ML) was found in Ref. 41 by observing peak ratios in Auger-electron spectroscopy.

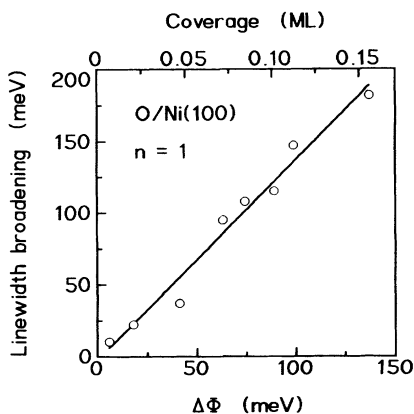


FIG. 3. Additional linewidth broadening $\Delta\Gamma$ of the first image state on Ni(100), induced by the adsorption of oxygen. The lower abscissa shows the adsorbate-induced increase in work function, $\Delta\Phi$. The absolute coverage Θ given in the upper abscissa was calculated from $\Delta\Phi$ using the data of Ref. 40.

Using these data we calculated the absolute coverage shown also in Fig. 3. Obviously a linear relationship between $\Delta\Gamma$ and Θ holds for this system, and we find an experimental slope of ≈ 1.2 eV/ML.

There are two possible mechanisms to explain the linewidth broadening: Scattering of the electron out of the image state (e.g., into bulk states) by the adsorbate atoms, and elastic scattering within the image state. The first process obviously is—at least for small coverages—proportional to the coverage. We are going to discuss the second process in more detail and show that it also results in a linewidth broadening proportional to the coverage.

The theoretical models of image states that have been discussed up to now assumed translational invariance parallel to the surface, which means that the image states have been assumed to be infinitely extended laterally. With disordered adsorption this translational invariance is weakened. At low coverage ($\ll 1$ ML) the adsorbed atoms cause a k_{\parallel} uncertainty Δk_{\parallel} which, according to the $E(k_{\parallel})$ dispersion, leads to a broadening of the image state. Adopting the view that the adatoms act as elastic scattering centers for electrons in image states and thus confine the state laterally, Δk_{\parallel} can be related via the uncertainty principle to the average nearest-neighbor distance of the adatoms: $\Delta k_{\parallel} a / \sqrt{\Theta} \approx 1$, where a^2 is the area of the unit cell of the clean surface and Θ the coverage. Detecting the electrons in normal emission, one finds then a linear dependence of the adsorbate-induced linewidth broadening on the coverage

$$\Delta\Gamma = \frac{\hbar^2}{2m^*} \frac{1}{a^2} \Theta. \quad (1)$$

From (1) a slope of ≈ 0.6 eV/ML is expected for adsorption on Ni(100). As compared to the experimental slope of 1.2 eV/ML this result gives the correct order of magnitude. Indeed the experimental value is larger, indicating the abovementioned additional scattering processes out of the image state, which reduce the lifetime of the image state and lead to a further linewidth broadening. Thus we were able to show for O/Ni(100) that simple theoretical considerations are compatible with the experimental adsorbate-induced linewidth broadening.

Our earlier results of adsorption experiments on Ag(100) and Ni(111) deserve to be mentioned here: For the system O/Ag(100) (Ref. 9) we also found an increase of linewidth with coverage but an evaluation like that for O/Ni(100) is not possible, since the work function change $\Delta\Phi(\Theta)$ is much less reproducible.⁴¹ Assuming a constant sticking coefficient, however, would indicate a nonlinear dependence of $\Delta\Gamma$ on Θ : $\Delta\Gamma \propto \sqrt{\Theta}$ for both the $n=1$ and $n=2$ states. This could in principle be related to an adsorption mode like, e.g., chain formation that does not produce a $\Delta k_{\parallel} \propto \sqrt{\Theta}$ as assumed in the derivation of (1). But since there is no evidence for this from, e.g., LEED experiments, an interpretation in terms of the onset of saturation in the sticking coefficient seems more appropriate.

In contrast to these results, which confirm the expected broadening effect, we found a decrease in linewidth upon adsorption of residual gas on Ni(111) (Ref. 10) from more

than 80 to about 70 meV. The contamination by the residual gas quenches the surface-state band and blocks a decay channel for the image state.

V. DISCUSSION

The experimental results for the linewidths of image states are summarized in Table I. $\Delta\Gamma$ denotes the change in linewidth upon adsorption, which is symbolized by up and down arrows. We are now going to make systematic comparisons between the different surfaces and between experiments and theoretical values also included in Table I.

We note first that the theoretical linewidths (8–40 meV) are in the same order of magnitude as the experimental ones (16–84 meV), despite the approximations in the present theory. Furthermore, even though the small linewidths for the $n=2$ states are difficult to determine accurately in our experiment, we could show for Ag(100), Ni(111), and Ni(100) that the lifetime broadening of the $n=2$ state is smaller than that of the respective $n=1$ state. This is also in accordance with theory. Long lifetimes can be measured better with time-resolved 2PPE using femtosecond laser pulses.^{15–17} There the linewidth of the $n=2$ image state for Ag(100) has been obtained to 3.7 ± 0.4 meV.¹⁶ Combining this value with our result 21 ± 4 meV for the $n=1$ state, where energy-resolved 2PPE is more accurate (see Table I), we note that the lifetime of the $n=2$ state is 5.7 ± 1.2 times longer than the lifetime of the $n=1$ state. This ratio differs significantly from the asymptotical n^3 expectation¹³ and is closer to the prediction 3.9 of Ref. 23.

For the more complicated discussion of the surface and material dependence of the $n=1$ state, Fig. 4(b) presents a graphic summary of the experimental and theoretical

linewidths on each material. The corresponding panels in 4(a) contain the k_{\parallel} -dependent projected bulk band structure— d bands emphasized by dark shading—as well as the crystal-induced surface states. For completeness Ag(111) is also included, the only other surface for which experimental data for the lifetimes of image states have been published.¹⁷

From this figure departures from the theoretical expectations which were mentioned in the preceding section are obvious. These deviations are explained by taking into account the effect of the actual band structure on the decay rate of image states. As outlined in Sec. II, present theory assumes free-electron-like states, which produce a smooth, but not particularly large density of states (DOS) around E_F , providing the decay channels for the image state. However, this may not be a good approximation of the electronic structure of the actual material: If E_F lies in a relative band gap, there are no direct decay channels for the image state, and the lifetime broadening should be much smaller than according to Echenique's free-electron theory. On the other hand, if there is a higher DOS above E_F than in free-electron-like bands, the additional decay channels lead to a larger lifetime broadening than in theory. We point out here that since the image state is located mainly in front of the surface the decay via electron-hole pair production is dominated by small k_{\parallel} transfer.²¹

For Cu(111) no unoccupied states exist between E_F and the first image state at $k_{\parallel}=0$. Such states exist only from $k_{\parallel} > 0.21 \text{ \AA}^{-1}$ on, where the $n=0$ surface state crosses E_F , dispersing upwards with an effective mass $m^*/m_e=0.46$.⁴² For $k_{\parallel} > 0.24 \text{ \AA}^{-1}$, where the gap edge crosses E_F , unoccupied bulk states can contribute as well to the decay. In contrast, Ag(100) has bulk sp states around E_F for $k_{\parallel}=0$ and is therefore more similar to a

TABLE I. Lifetime broadening Γ of image states on metals. The first row shows the experimental linewidths for the first image state, the second row theoretical estimates within Echenique's free-electron theory. The response of Γ upon disordered adsorption in the submonolayer regime is denoted by arrows in the next row. These results can be explained by the density of states (DOS) above E_F (see text). The main contribution (around $k_{\parallel}=0$) to the actual DOS is shown in the fourth row; an SS there denotes an unoccupied surface state. The last row contains the experimental results for the second image state.

	Ag(100)	Cu(111)	Ni(100)	Ni(111)	Ag(111)
Γ_1^{expt} (meV)	21 ± 4^a $19\dots 44^d$	16 ± 4^b	70 ± 8^b	84 ± 10^c	$> 33^c$ ≈ 20
Γ_1^{theor} (meV) ^f	8	≈ 40	≈ 15	≈ 15	≈ 20
$\Delta\Gamma$ (adsorption)	\nearrow		\nearrow	\searrow	
DOS (above E_F)	sp bands	0	d bands	d bands + SS	0 + SS for small k_{\parallel}
Γ_2^{expt} (meV)	5 ± 5^a 3.7 ± 0.4^g			12 ± 10^c	

^a Energy-resolved 2PPE experiments (Ref. 9).

^b Energy-resolved 2PPE experiments (this work).

^c Energy-resolved 2PPE experiments (Ref. 10).

^d Time-resolved 2PPE experiments (Ref. 15).

^e Time-resolved 2PPE experiments (Ref. 17).

^f Theory: Refs. 19 and 22, and extrapolation (see text).

^g Time-resolved 2PPE experiments (Ref. 16).

free-electron-like metal. This shows that the effect of the larger penetration of the image-state wave function on Cu(111) is more than compensated for by the lack of DOS at E_F around $k_{\parallel}=0$. The theoretical trend in lifetime broadening is therefore opposite to the experiment.

On the nickel surfaces the deviation from the free-electron theory is at least as large as on Cu(111). In this case however, a larger lifetime broadening is observed. Here the second argument from above can be applied: On nickel the d bands are located around E_F and lead to a high DOS compared to free-electron bands, which in turn provides more decay channels than accounted for in Echenique's theory. Moreover, in Ref. 10 we concluded from the decrease in linewidth of ≈ 15 meV upon low-coverage adsorption on Ni(111) that the unoccupied crystal-induced surface state present on this surface must also act as an additional decay channel. On adsorption this decay channel is quenched, which explains the decrease in linewidth. On Ni(100) an unoccupied surface resonance exists in the continuum of the free-electron-like sp bands. Within our experimental errors we did not

observe an initial decrease of the linewidth upon oxygen adsorption (see Fig. 3). Possible explanations are that the quenching of the surface resonance proceeds slowly with increasing oxygen coverage or that the more bulklike character of the surface resonance makes it a less probable decay channel compared to a true surface state as on Ni(111). Table I summarizes all these explanations of how the band structure affects the image-state lifetime in short form.

We would also like to discuss the experimental results for the linewidth on Ag(111) also given in Table I and Fig. 4 within this picture. There exist experimentally determined upper and lower limits for the linewidth on this surface: $\Gamma_1^{\text{Ag}(111)} > 33$ meV from time-resolved 2PPE,¹⁷ and < 80 meV from early energy-resolved 2PPE.⁵ For Ag(111) the band gap extends below E_F , and thus one could expect—just like for Cu(111)—a smaller linewidth than the 20 meV from free-electron-like theory. The effect should be less pronounced than on Cu(111), since unoccupied bulk states exist for smaller k_{\parallel} ($> 0.22 \text{ \AA}^{-1}$). However, quite unlike the situation on Cu(111), the crystal-induced surface state S_0 on Ag(111) is located only 50 meV below E_F at $k_{\parallel}=0$ (Ref. 28) and is therefore at room temperature partially unoccupied even for $k_{\parallel}=0$. Due to its large overlap with the image-state wave function this forms an efficient additional decay channel that leads to the relatively large linewidth for this surface.

VI. PROSPECTS OF 2DEG PHYSICS WITH IMAGE STATES

Finally, we want to comment on using electrons in image states as a realization of a two-dimensional electron gas (2DEG) in vacuum with a simple holding potential. The vision of “exciting two-dimensional electron-gas physics”⁴³ on the basis of image states is indeed very tempting and therefore quite frequently encountered in the literature about image states, e.g., in Refs. 5, 6, 8, 21, 24, and 44.

In our work we use two ways for estimating the electron density \bar{n} in the first image state that was produced in our experiments:

(i) From the light intensity for the *first excitation step* an upper limit for \bar{n} follows easily

$$\bar{n} \leq \frac{1}{A} \frac{W_p}{2h\nu} \frac{\tau}{\Delta t_p}, \quad (2)$$

where W_p and Δt_p denote energy and length of the laser pulse, A the illuminated area, and τ the lifetime of the image state. Of course equality in (2) holds only if each incoming photon excites an electron into the image state, and densities several orders of magnitude lower are more realistic. Plugging into (2) a maximum usable intensity $(W_p/A)_{\text{max}} \approx 1 \text{ mJ/cm}^2$ and the maximum image-state lifetime $\tau \approx 40 \text{ fs}$ we obtain the strict upper limit for the electron density $\bar{n} < 4 \times 10^9 \text{ cm}^{-2}$.

(ii) The light-induced transition rate γ_1 for the *second excitation step* in 2PPE was approximately calculated in Ref. 45 and can be used for an estimate of \bar{n} as well:

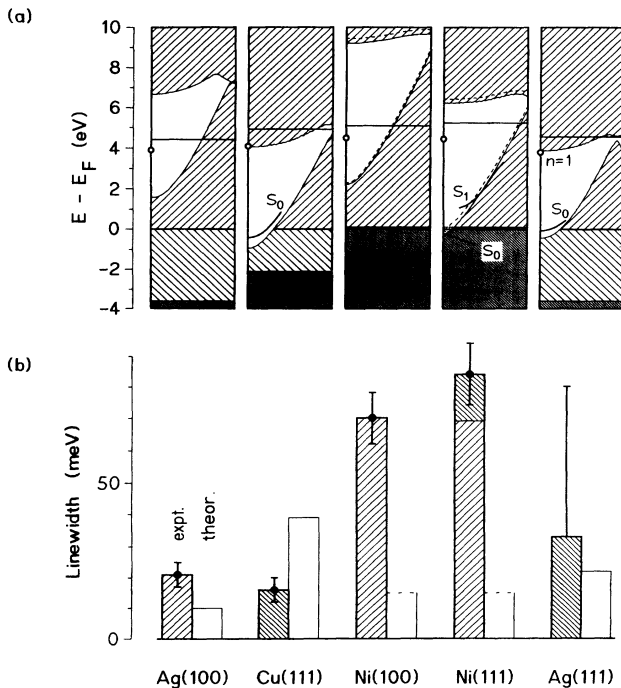


FIG. 4. Linewidth of the first image state on metals. (a) Projected bulk band structure for each face. On each panel k_{\parallel} is drawn to the right, running from 0.0 to 1.0 \AA^{-1} along the $\Gamma\text{-}\bar{M}$ direction. The $n=1$ image state for $k_{\parallel}=0$ is shown as a circle. The crystal-induced surface states are denoted by S_0 and S_1 . The darker areas indicate the position of the d bands (disregarding their k_{\parallel} dependence). In addition, on the Ni faces the ferromagnetic splitting of the bulk band gap is shown by the dashed lines. (b) Comparison between experimental results of this work [Ag(100), Cu(111), Ni(100), and Ni(111)] and the present theory (after Ref. 22). The experimental values for Ag(111) are taken from time-resolved 2PPE (Ref. 17) (lower limit) and earlier 2PPE (Ref. 5) (upper limit). The darker shading of the experimental histogram for the (111) surfaces indicates the effect of surface states on the linewidth of the $n=1$ state on these surfaces.

$$\gamma_1 = \alpha' F(\eta) E^2,$$

$$\text{with } \alpha' = 2^{15} \pi m_e e^2 a_0^4 \beta^2 / \hbar^3 \quad (3)$$

$$\text{and } F(\eta) = e^{-4\eta \tan^{-1}(\eta^{-1})} / [(1 - e^{-2\pi\eta})(1 + \eta^{-2})^4],$$

where $\eta = 1/4ka_0$, $k = \sqrt{2m_e E_{\text{kin}}/\hbar^2}$, $\beta \approx 1/\sqrt{2}$ in our setup. E is the amplitude of the incident electromagnetic field and is related to the intensity by $E^2 = W_p / (\epsilon_0 c A \Delta t_p)$. By introducing the energy-integrated number of electrons N detected in the image peak and taking into account the finite angular resolution Δk_{\parallel} one obtains

$$\bar{n} = N \frac{2h\nu - \Phi + |E_b|}{(\hbar^2/2m^*)(\Delta k_{\parallel})^2 \alpha F(\eta) W_p}, \quad (4)$$

with $\alpha = \alpha' / \epsilon_0 c \approx 30 \text{ cm}^2/\text{mJ}$. From (4) we find electron densities in the range 5×10^5 to $5 \times 10^6 \text{ cm}^{-2}$ in our experiments. With the density of states of a 2DEG $D(E) = m^* / (\pi \hbar^2)$, and assuming thermalization, these electron densities correspond to a Fermi energy in the eV range. Obviously the image-state electron gas in front of a metal surface is too short lived to exhibit Fermi statistics within the constraints of this experiment. In semiconductor physics densities of 10^{12} cm^{-2} (and $m^* \approx 0.1m_e$) are typical for 2DEG experiments.⁴⁶

Using higher intensities for the first excitation step would give proportionally increased densities; the sample temperature, however, is increased as well. An experimentally verified estimate for the temperature rise caused by nanosecond laser pulses, which is based on a thermal diffusion *ansatz*, can be found in Ref. 47. On the other hand, shorter pulse lengths Δt_p increase the electron density like $1/\Delta t_p$, but the sample temperature after Ref. 48 only like $1/\sqrt{\Delta t_p}$. Extrapolating the thermal diffusion model to femtosecond pulses would indicate that an electron density 10^3 times that obtained in our experiments could be possible. However, this model neglects that femtosecond pulses act mainly on raising the temperature of the metal electrons, not that of the lattice, a process that again raises the threshold for observing Fermi statistics in the image state. To summarize these ideas we note that a two-dimensional Fermi gas does not seem to be attainable and observable at the same time in a 2PPE experiment.

VII. SUMMARY AND OUTLOOK

In this paper we have presented the first systematic study of intrinsic linewidths of image-potential states on metal surfaces, a task which was made possible by the recent progress in high-resolution bichromatic two-photon photoemission spectroscopy. By comparing the results to predictions of the present theory we find that it is not sufficient to account only for free-electron states of the metal. Details of the actual band structure, however, can explain the discrepancies between experiment and theory quite easily: Lacking DOS near $k_{\parallel} = 0$ explains the unexpectedly small linewidth on Cu(111). The large unoccupied DOS due to d bands leads to the large linewidths observed on nickel. Recent experiments on Fe(110) and Co(0001) follow the same trend.⁴⁸ We would like to point out that for the d -band metals the predictions for the image-state energies are in much poorer agreement with the experimental values than for free-electron-like metals.^{49,33} A possible reason for this might be that for the metals with partially filled d shells we have a large self-energy correction for the real part as well as for the imaginary part. The latter is measured in our experiment directly, whereas the former is seen only as a shift in binding energy. An unoccupied surface state like on Ni(111) further broadens the image state and leads to an anomalous behavior upon adsorption. Disordered adsorption on Ni(100) can be understood semiquantitatively simply by taking the adatoms as scattering centers confining the lateral extension of image states parallel to the surface.

Even though it seems impossible to investigate two-dimensional electron-gas physics in 2PPE experiments, our estimates give information about the laser intensities necessary for pumping a significant electron density into the image state. It remains a difficult task to do this without heating the surface and the electron gas too much, and to devise an experiment which permits the observation of the two-dimensional electron gas at the same time.

Another interesting problem which deserves further investigation is the question whether a coherent excitation process can be observed in 2PPE experiments. This would require an initial state very close to E_F which lives longer than the image state.

ACKNOWLEDGMENT

Financial support by the Deutsche Forschungsgemeinschaft is gratefully acknowledged.

¹A. Adnot and J. D. Carette, Phys. Rev. Lett. **38**, 1084 (1977).
²V. Dose, W. Altmann, A. Goldmann, U. Kolac, and J. Rogozik, Phys. Rev. Lett. **52**, 1919 (1984).
³D. Straub and F. J. Himpsel, Phys. Rev. Lett. **52**, 1922 (1984).
⁴P. D. Johnson and N. V. Smith, Phys. Rev. B **27**, 2527 (1983).
⁵K. Giesen, F. Hage, F. J. Himpsel, H. J. Riess, and W. Steinmann, Phys. Rev. Lett. **55**, 300 (1985).
⁶W. Steinmann, Appl. Phys. A **49**, 365 (1989).
⁷V. Dose, Th. Fauster, and R. Schneider, Appl. Phys. A **40**, 203 (1986).

⁸F. J. Himpsel, Phys. Rev. B **43**, 13 394 (1991).
⁹S. Schuppler, N. Fischer, Th. Fauster, and W. Steinmann, Appl. Phys. A **51**, 322 (1990).
¹⁰N. Fischer, S. Schuppler, Th. Fauster, and W. Steinmann, Phys. Rev. B **42**, 9717 (1990).
¹¹S. Schuppler, Ph.D. thesis, University of Munich, 1991.
¹²N. V. Smith, Phys. Rev. B **32**, 3549 (1985).
¹³P. M. Echenique and J. B. Pendry, J. Phys. C **11**, 2065 (1978).
¹⁴K. Giesen, F. Hage, F. J. Himpsel, H. J. Riess, and W. Steinmann, Phys. Rev. B **35**, 971 (1987).

- ¹⁵R. W. Schoenlein, J. G. Fujimoto, G. L. Eesley, and T. W. Capehart, *Phys. Rev. Lett.* **61**, 2596 (1988).
- ¹⁶R. W. Schoenlein, J. G. Fujimoto, G. L. Eesley, and T. W. Capehart, *Phys. Rev. B* **41**, 5436 (1990).
- ¹⁷R. W. Schoenlein, J. G. Fujimoto, G. L. Eesley, and T. W. Capehart, *Phys. Rev. B* **43**, 4688 (1991).
- ¹⁸W. Altmann, Ph.D. thesis, University of Würzburg, 1988; A. Goldmann, W. Altmann, and V. Dose, *Solid State Commun.* **79**, 511 (1991).
- ¹⁹P. M. Echenique, F. Flores, and F. Sols, *Phys. Rev. Lett.* **55**, 2348 (1985).
- ²⁰A. G. Eguluz and W. Hanke, *Phys. Rev. B* **39**, 10433 (1989).
- ²¹P. M. Echenique and J. B. Pendry, *Prog. Surf. Sci.* **32**, 111 (1990).
- ²²P. de Andres, P. M. Echenique, and F. Flores, *Phys. Rev. B* **35**, 4529 (1987).
- ²³P. L. de Andres, P. M. Echenique, and F. Flores, *Phys. Rev. B* **39**, 10356 (1989).
- ²⁴P. M. Echenique and M. E. Uranga, *Surf. Sci.* **247**, 125 (1991).
- ²⁵L. Hedin and S. Lundqvist, in *Solid State Physics*, edited by F. Seitz, D. Turnbull, and H. Ehrenreich (Academic, New York, 1969), Vol. 23, p. 1.
- ²⁶R. H. Ritchie and A. L. Marusak, *Surf. Sci.* **4**, 234 (1966).
- ²⁷J. Lindhard, *Dan. Mat. Fys. Medd.* **28**, 1 (1954).
- ²⁸K. Giesen, F. Hage, F. J. Himpsel, H. J. Riess, and W. Steinmann, *Phys. Rev. B* **33**, 5241 (1986).
- ²⁹M. Ortuno and P. M. Echenique, *Phys. Rev. B* **34**, 5199 (1986).
- ³⁰R. Courths and S. Hufner, *Phys. Rep.* **112**, 53 (1984).
- ³¹G. D. Kubiak, *Surf. Sci.* **201**, L475 (1988).
- ³²K. Giesen, F. Hage, F. J. Himpsel, H. J. Riess, W. Steinmann, and N. V. Smith, *Phys. Rev. B* **35**, 975 (1987).
- ³³S. Schuppler, N. Fischer, W. Steinmann, R. Schneider, and E. Bertel, *Phys. Rev. B* **42**, 9403 (1990).
- ³⁴D. N. Nikogosyan, *Appl. Phys. A* **52**, 359 (1991).
- ³⁵R. E. Imhof, A. Adams, and G. C. King, *J. Phys. E* **9**, 138 (1976). In our setup the relative pencil angle α/α_0 is $\approx \frac{1}{2}$. The angle α_0 , which is defined in that work as $\sqrt{d/4r_0}$, is about 4.7° in our experiment.
- ³⁶J. B. Pendry, in *Photoemission and the Electronic Properties of Surfaces*, edited by B. Feuerbacher, B. Fitton, and R. F. Willis (Wiley, Chichester, 1978).
- ³⁷J. Tersoff and S. D. Kevan, *Phys. Rev. B* **28**, 4267 (1983).
- ³⁸F. J. Himpsel and D. E. Eastman, *Phys. Rev. Lett.* **41**, 507 (1978).
- ³⁹K. Starke, K. Ertl, and V. Dose, *Phys. Rev. B* **45**, 6154 (1992).
- ⁴⁰J. E. Demuth and T. N. Rhodin, *Surf. Sci.* **45**, 249 (1974).
- ⁴¹H. A. Engelhardt and D. Menzel, *Surf. Sci.* **57**, 591 (1976).
- ⁴²S. D. Kevan, *Phys. Rev. Lett.* **50**, 526 (1983).
- ⁴³F. J. Himpsel, in *Chemistry and Physics of Solids Surfaces VI*, edited by R. Vanselow and R. Howe (Springer, Berlin, 1986).
- ⁴⁴K. Giesen, F. Hage, H. J. Riess, W. Steinmann, R. Haight, R. Beigang, R. Dreyfus, Ph. Avouris, and F. J. Himpsel, *Phys. Scr.* **35**, 578 (1987).
- ⁴⁵R. Shakeshaft and L. Spruch, *Phys. Rev. A* **31**, 1535 (1985).
- ⁴⁶T. Ando, A. B. Fowler, and F. Stern, *Rev. Mod. Phys.* **54**, 437 (1982).
- ⁴⁷J. E. Hicks, L. E. Urbach, E. W. Plummer, and H.-L. Dai, *Phys. Rev. Lett.* **61**, 2588 (1988).
- ⁴⁸R. Fischer, N. Fischer, S. Schuppler, Th. Fauster, and F. J. Himpsel, *Phys. Rev. B* **46**, 9691 (1992).
- ⁴⁹N. V. Smith, C. T. Chen, and M. Weinert, *Phys. Rev. B* **40**, 7565 (1989).

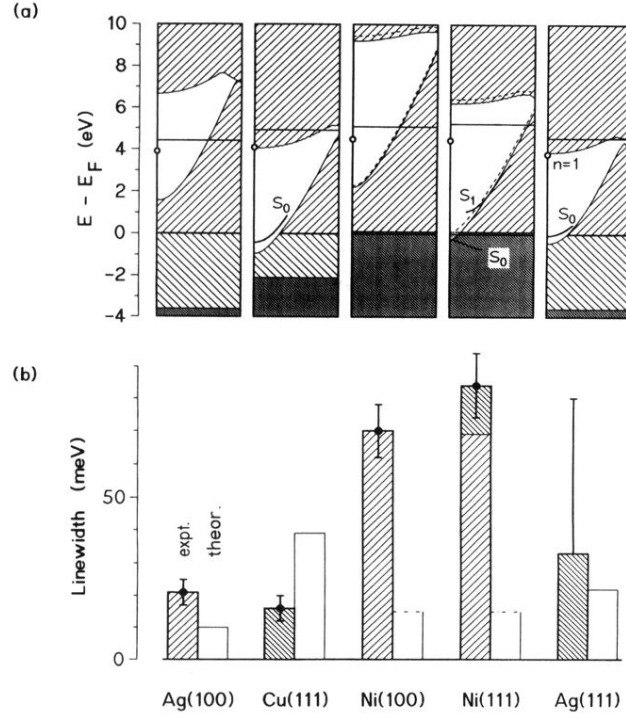


FIG. 4. Linewidth of the first image state on metals. (a) Projected bulk band structure for each face. On each panel k_{\parallel} is drawn to the right, running from 0.0 to 1.0 \AA^{-1} along the $\Gamma\text{-}\bar{M}$ direction. The $n=1$ image state for $k_{\parallel}=0$ is shown as a circle. The crystal-induced surface states are denoted by S_0 and S_1 . The darker areas indicate the position of the d bands (disregarding their k_{\parallel} dependence). In addition, on the Ni faces the ferromagnetic splitting of the bulk band gap is shown by the dashed lines. (b) Comparison between experimental results of this work [Ag(100), Cu(111), Ni(100), and Ni(111)] and the present theory (after Ref. 22). The experimental values for Ag(111) are taken from time-resolved 2PPE (Ref. 17) (lower limit) and earlier 2PPE (Ref. 5) (upper limit). The darker shading of the experimental histogram for the (111) surfaces indicates the effect of surface states on the linewidth of the $n=1$ state on these surfaces.